An Unstructured Finite Volume Model for Dam-break Floods with Wet/dry Fronts

Jinbo Yang
Ph. D., Department of Hydraulics Research, Changjiang River Scientific Research Institute, Wuhan, Hubei, 430010, China, E-mail:yangjb1225@163.com

Wengang Duan
M. E., S. E., Department of Hydraulics Research, Changjiang River Scientific Research Institute, Wuhan, Hubei, 430010, China, E-mail:ckydwg@163.com

Siying Wang
Ph. D., Department of Hydraulics Research, Changjiang River Scientific Research Institute, Wuhan, Hubei, 430010, China, E-mail: thing@ustc.edu

Dingfang Li
Professor, School of Mathematics and Statistics, Wuhan University, Wuhan, Hubei, 430072, China, E-mail:dfli@whu.com.cn

ABSTRACT: In this paper, A well-balanced Godunov-type scheme for the 2D shallow water flow is proposed to model the dam-break floods with irregular topography and wet/dry fronts on the triangular mesh. Here, the HLLC Riemann solver is applied to approximate the intercell numerical flux at each interface with the rectangle formula employed to approximate the line integral of the bed slope terms along the sides of each element. In order to obtain a second-order accurate numerical scheme, the MUSCL data reconstruction and Runge-Kutta are applied in the space and time, respectively. For the wet/dry fronts, the redefinition of the discretized bottom function is applied at the wet/dry transitions. Finally, the tests of dam-break floods with irregular topography and wet/dry fronts are simulated, of which of the results are in good agreement with the analytical solutions and existing results.

KEY WORDS: Shallow Water Equations, Well-balanced, Dam break, Wet/dry fronts, HLLC Riemann solver.

1 INTRODUCTION

The free-surface shallow water flow is a popular physical phenomenon in hydrodynamics such as oceans, open channels, and dam break problem, which can be modeled by the shallow water equations. Due to the properties of nonlinearity and hyperbolicity, the shallow water equations often admit the discontinuous solutions with hydraulic jumps and bores. In practice, the shallow water flows are also always associated with the complex geometry region and irregular topography. Therefore, it is essential to construct appropriate numerical schemes to simulate the shallow water equations to predict the complicated shallow water flows in hydraulic engineering. The Godunov-type finite volume schemes (Godunov, 1959) are a kind of upwind and conservative numerical schemes, which can capture the shock waves of the conservation laws，so that the Godunov-type schemes have been extended to the shallow water equations by some researchers (Alcrudo et al, 1993, Zhao et al, 1996, Delis et al, 2000) to simulate dam break problem and flooding waves with wet/dry fronts. The treatment of source terms is a challenging issue. Roe(Roe, 1986)proposes the idea of upwind for source terms in the conservation laws. LeVeque(LeVeque, 1998) adopts the Quasi-Steady Wave-Propagation Algorithm to obtain a balanced scheme by introducing a local Riemann problem in the center of each cell. Zhou et al(Zhou et al, 2001) propose the surface gradient method(SGM) for the 2D nonhomogeneous shallow water equations over the irregular topography, which is suitable for the steady and quasi-steady flows and satisfies C-property. Xing and Shu (Xing et al, 2006) propose a well balanced high order weighted essentially non-oscillatory finite volume scheme(WENO) for the shallow water equations. At the same time, the treatment of wet/dry

fronts is another challenging difficulty. For the treatment of the wet/dry front, a new technique of treating wet/dry fronts based on the context of the Roe scheme has been presented by redefining the discretized bottom function. The improvement of the treatment of dry interface is performed in (Castro et al, 2005) by modifying the state values at the wet/dry fronts to improve the accuracy of the velocity of the advancing wet/dry fronts. In this work, a well-balanced second order accurate finite volume scheme is proposed for the 2D shallow water equations based on the triangular mesh. Several tests of dam-break issue are simulated, of which the results demonstrate that the numerical scheme is high resolution, well-balanced and can deal with wet/dry fronts in the realistic engineering.

2 GOVERNING EQUATIONS AND NUMERICAL SCHEME

2.1 Shallow Water Equation

The 2D shallow water equations with source terms arising from the bed profile and bed friction can be used for the free surface shallow flows, which read in the conservation laws

$$\frac{\partial \mathrm{U}}{\partial t}+\frac{\partial F}{\partial x}+\frac{\partial G}{\partial y}=S \tag{1}$$

with the vectors given by, respectively

$$U=\begin{pmatrix} H \\ q_x \\ q_y \end{pmatrix},\ F=\begin{pmatrix} q_x \\ \frac{q_x^2}{h}+\frac{1}{2}gH^2-gbH \\ \frac{q_x q_y}{h} \end{pmatrix},\ G=\begin{pmatrix} q_y \\ \frac{q_x q_y}{h} \\ \frac{q_y^2}{h}+\frac{1}{2}gH^2-gbH \end{pmatrix},\ S=S_b+S_f=\begin{pmatrix} 0 \\ -gH\frac{\partial b}{\partial x} \\ -gH\frac{\partial b}{\partial y} \end{pmatrix}+\begin{pmatrix} 0 \\ -\frac{g}{\rho}\tau_{fx} \\ -\frac{g}{\rho}\tau_{fy} \end{pmatrix} \tag{2}$$

where t accounts for the time independent variable, and x, y represent the spatial independent variables. The quantity H denotes the water surface elevation and b is the bed elevation. H=h+b where the scale h denotes the water depth. g is the acceleration due to the gravity. ρ is the water density. q_x=hu and q_y=hv, where u and v are respectively depth average components of the velocity $\vec{u}=[u,v]$ in the x and y directions, are the per unit width water discharges. The vectors F(U) and G(U) are the flux vectors in the x and y directions, respectively. In source terms, the notation s_b denotes the bed slope term and s_f is the bed shear stress term with the quantities τ_{fx}, τ_{fy} defined by the following empirical formulae

$$\tau_{fx}=\rho C_f u\sqrt{u^2+v^2}\ ,\quad \tau_{fy}=\rho C_f v\sqrt{u^2+v^2} \tag{3}$$

where the bed friction coefficient estimated by $C_f=gn_m^2/h^{1/3}$ with n being the manning coefficient.

2.2 Numerical scheme

Based on the triangular mesh in Fig 1, the state solutions may be updated with the marching time by the following conservative numerical scheme in the finite volume scheme.

$$\frac{\partial \mathrm{U}_i}{\partial t}+\frac{1}{|V_i|}\sum_{j=1}^{M}\int_{L_j}\cos\theta_j F(U)+\sin\theta_j \mathrm{G}(U)d\varsigma=\frac{1}{|V_i|}S_i \tag{4}$$

where V_i is the cell area. M is the total of sides of the corresponding element, M=3 for the triangular element. ς_j is the cell side length. The notation $n=\left[n_x,n_y\right]=\left[\cos\theta,\sin\theta\right]$ presents the outward unit

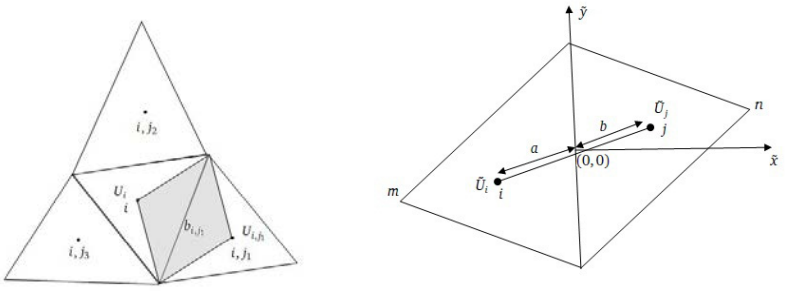

Figure 1 the computational mesh and the local coordinate

normal vector to the interface, where the quantity θ is the angle between the vector n and the positive x direction. The quantity U_i is defined by the integral average of the solution over the corresponding element, $U_i = \frac{1}{|V_i|}\iint_{V_j} U(x,y,t)dV$, And $\overline{S}$ is the numerical source terms $S_i = \frac{1}{|V_i|}\iint_{V_j} S(x,y,U)dV$. $E_{i,j}(U)\cdot n_{i,j}$ is the normal flux vector defined by, using the rotational invariance property of the 2D shallow water equations

$$E(U)\cdot n = \cos\theta F(U) + \sin\theta G(U) = T^{-1}(\theta)F(T(\theta)U) = T^{-1}(\theta)F(\tilde{U}) \tag{5}$$

Here $\tilde{U} = T(\theta)U$, and $T(\theta)$ and $T^{-1}(\theta)$ are the rotation matrix and the corresponding inverse rotation matrix given, respectively

$$T(\theta) = \begin{pmatrix} 1 & 0 & 0 \\ 0 & \cos\theta & \sin\theta \\ 0 & -\sin\theta & \cos\theta \end{pmatrix}, T^{-1}(\theta) = \begin{pmatrix} 1 & 0 & 0 \\ 0 & \cos\theta & -\sin\theta \\ 0 & \sin\theta & \cos\theta \end{pmatrix} \tag{6}$$

Therefore, to develop a numerical scheme, the approximations to the intercell flux $F_i(\overline{U})$ at each interface and the source terms S_i in each element must be determined. The transformed quantity $\tilde{U}$, arising from the original variable U, is discontinuous across the interface between two neighboring elements, since the quantity U can have different values in different elements. Therefore, the procedure of obtaining the intercell numerical flux can be translated to solving a series of one dimensional Riemann problems in the local reference coordinate with x-axis normal to the interface side and the origin locating in the midpoint of the corresponding side, as in Fig 2.

$$\tilde{U}_t + F(\tilde{U})_{\tilde{x}} = 0, \quad \tilde{U}(\tilde{x},0) = \begin{cases} \tilde{U}_L & \tilde{x} < 0 \\ \tilde{U}_R & \tilde{x} > 0 \end{cases} \tag{7}$$

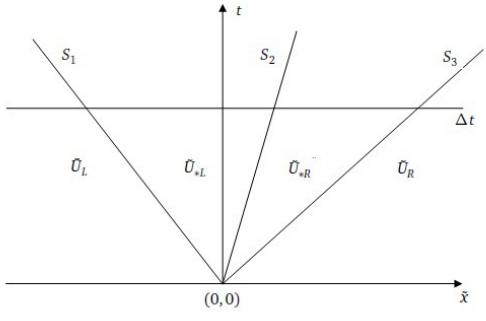

Figure 2 The evaluation of HLLC numerical flux for 2D shallow water equations.

In end, the finite volume scheme is given by

$$U_i^{n+1} = U_i^n - \frac{\Delta t}{|V_j|}\sum_{j=1}^{3} T^{-1}(\theta)F(\tilde{U})\zeta_j + \frac{\Delta t}{|V_j|}S_j \tag{8}$$

2.2.1 HLLC Riemann solver

Here, the HLLC (Toro, 2001) approximate Riemann solver is performed for the intercell numerical flux $F(U)$, which can be given simplified by the HLL solver as follows

$$\left[F^{hllc}\right]_{(k)} = \left[F^{hll}\right]_{(k)}, k = 1,2,\ \left[F^{hllc}\right]_{(3)} = \begin{cases} \left[F^{hllc}\right]_{(1)} v_L & S_2 > 0 \\ \left[F^{hllc}\right]_{(1)} v_R & S_2 < 0 \end{cases} \tag{9}$$

where the subscript (k) represents the k-th component of the flux vector and the HLL numerical flux is defined as

$$F^{HLL} = \begin{cases} F_L & S_1 \geq 0 \\ \dfrac{S_2 F_L - S_1 F_R + S_1 S_2 (U_R - U_L)}{S_2 - S_1} & S_1 < 0 < S_2 \\ F_R & S_2 \leq 0 \end{cases} \tag{10}$$

The left and right waves propagation speeds S_1,S_3 are given by, respectively

$$S_1 = \min(\tilde{u}_L - \sqrt{gh_L}, u_s - \sqrt{gh_s}), \quad S_3 = \max(\tilde{u}_R + \sqrt{gh_R}, u_s + \sqrt{gh_s}) \tag{11}$$

In which

$$u_s = (u_i + u_{i+1})/2 + \sqrt{gh_i} - \sqrt{gh_{i+1}} \quad \text{and} \quad \sqrt{gh_s} = (\sqrt{gh_i} + \sqrt{gh_{i+1}})/2 + (u_i - u_{i+1})/4 \tag{12}$$

For the intermediate wave speed S_2 (Toro, 2001),

$$S_2 = \frac{S_1 h_L \left(\tilde{u}_R - S_3\right) - S_3 h_R \left(\tilde{u}_L - S_1\right)}{h_L \left(\tilde{u}_R - S_3\right) - h_R \left(\tilde{u}_L - S_1\right)} \tag{13}$$

In order to make the scheme suitable for the wet/dry bed problem, we shall modify the left wave speed S_1 and the right wave speed S_3 as follows

$$S_1 = u_{i+1} - 2\sqrt{gh_{i+1}}, \quad S_3 = u_{i+1} + \sqrt{gh_{i+1}} \quad \text{(right dry bed)} \tag{14}$$

$$S_1 = u_i - \sqrt{gh_i}, \quad S_3 = u_i + 2\sqrt{gh_i} \quad \text{(left dry bed)} \tag{15}$$

It is clear that the estimate S_2, given in (13), coincides with the dry front in (14) or (15).

2.2.2 The choice of the time step

In order to keep the numerical solution stable, the time step Δt must be adjusted at each time level and is given by

$$\Delta t = CFL \min_{1 \leq i \leq M} \min_{1 \leq j \leq 3} \frac{\min\left(\Delta x_{i,j,1}, \Delta x_{i,j,2}\right)}{\max\left(S_{i,j,1}, S_{i,j,2}\right)} \tag{16}$$

where CFL is the Courant number satisfying $0 < CFL \leq 1$.

2.2.3 MUSCL Data reconstruction

In order to obtain second-order accuracy in space, the MUSCL data reconstruction is performed. The value of state variables in the adjacent cells are given by

$$\tilde{U}_L = \tilde{U}_i + 0.5\delta\tilde{U}_L, \quad \tilde{U}_R = \tilde{U}_j + 0.5\delta\tilde{U}_R \tag{17}$$

where $\delta\tilde{U}_L$ and $\delta\tilde{U}_R$ are normal gradients of the state variables at the left and right hand sides of the edge, respectively, defined by

$$\delta\tilde{U}_L = G\left(\frac{2b}{a+b}\left(\tilde{U}_j-\tilde{U}_i\right),\left(\tilde{U}_i-\tilde{U}_m\right)\right), \delta\tilde{U}_R = G\left(\frac{2b}{a+b}\left(\tilde{U}_j-\tilde{U}_i\right),\left(\tilde{U}_n-\tilde{U}_j\right)\right) \tag{18}$$

where the definitions of a and b are shown in Fig. 1. The state values U_m and U_n at the points m and n can be evaluated by the mean value of the neighboring cells. The function G(a,b) is the slope limiter in (Toro, 2001), which can keep the scheme free from the spurious oscillations based on the reconstructed data.

At the same time, second order Runge-Kutta integration are performed for time.

2.3 The treatment of the source term

As previous consideration, it is very important to discretise source terms associated with topography to develop a well-balanced numerical scheme. Here the second component of source terms associated with topography in equation (1) is treated as follows

$$\iint_{V_i} gH\frac{\partial b}{\partial x}dxdy = -gH\iint_{V_i}\frac{\partial b}{\partial x}+\frac{\partial 0}{\partial x}dxdy = -gH\oint_{\zeta}(b,0)\cdot nd\zeta = -gH\sum_{i=1}^{3}\oint_{\zeta_i}(b_j,0)\cdot n_j d\zeta = -gH\sum_{i=1}^{3}b_j\cos\theta_j\zeta_j \tag{19}$$

For the third component of source terms

$$\iint_{V_i} gH\frac{\partial b}{\partial y}dxdy = -gH\iint_{V_i}\frac{\partial 0}{\partial x}+\frac{\partial b}{\partial y}dxdy = -gH\oint_{\zeta}(0,b)\cdot nd\zeta = -gH\sum_{i=1}^{3}\oint_{\zeta_i}(0,b_j)\cdot n_j d\zeta = -gH\sum_{i=1}^{3}b_j\sin\theta_j\zeta_j \tag{20}$$

2.4 Wet/Dry Fronts

In order to modify the numerical scheme for wet/dry fronts, we consider the interface $\ell_{i,j}$ connecting the wet element V_i and the dry element V_j. The modifications for the discretized bottom function, the state values for the dry element V_j and the each term of the numerical source terms arising from the topography are following, in Fig. 3.

$$b_{i,j} = H_i, \bar{S}_{i,j} = \begin{cases} \begin{pmatrix} 0 \\ -gH_iH_i\cos\theta_{i,j}\zeta_{i,j} \\ -gH_iH_i\sin\theta_{i,j}\zeta_{i,j} \end{pmatrix} & H_i > b_{i,j}, H_j < b_{i,j} \\ \begin{pmatrix} 0 \\ -gH_iH_i\cos\theta_{i,j}\zeta_{i,j} \\ -gH_iH_i\sin\theta_{i,j}\zeta_{i,j} \end{pmatrix} & otherwise \end{cases} \tag{21}$$

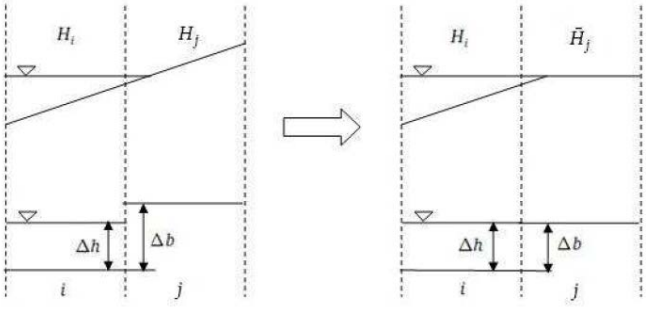

Figure 3 Redefinition of the discretized bottom with wet/dry fronts over adverse steep slopes

For the treatment of the moving water flows, we apply the technique for wet/dry fronts proposed in (Castro, 2005). Let us consider the above case with the emerging bottom at interface $I_{i,j}$ connecting the wet cell V_i and dry cell V_j. Then, we have

（1）Computing the modified numerical source terms along each side of the element V_i given by (21).

（2）Defining two states at interface $I_{i,j}$, $\tilde{U}_i^n = \begin{bmatrix} H_i^n \\ 0 \\ 0 \end{bmatrix}$ and $\tilde{U}_j^n = \begin{bmatrix} H_i^n \\ 0 \\ 0 \end{bmatrix}$.

（3）Updating the state U_i^{n+1} by using the intercell flux $F_{i,j}^{hllc}$ associated with states $\tilde{U}_i^n$ and $\tilde{U}_j^n$ and the modified source terms.

The treatment of wet/dry fronts is similar for the situation with the dry cell V_i and the wet cell V_j. The proposed numerical scheme is not modified when no bottom emergence occurs.

3 NUMERICAL TESTS

In this section, several tests of dam-break problem over the complex topography are simulated by the proposed numerical scheme. The tests show that the proposed numerical scheme has the ability of capturing shock waves sharply in the flows with the irregular topography and can deal with wet/dry fronts in realistic engineering.

3.1 Dam Break Problem Over a Step-like Bottom

A classical non-steady flow (Vignoli, 2008) is the dam break problem in the 16m-long channel with a step-like bed profile given by

$$b(x) = \begin{cases} 1m & 25/3 < x < 12.5 \\ 0 & otherwise \end{cases} \tag{22}$$

with the initial conditions set by H_0=10-b(x) and $Q_0 = \begin{cases} 350m^3/s & x > 50/3 \\ -350m^3/s & otherwise \end{cases}$.

The physical domain is partitioned into 500 cells and CFL=0.8. When t=1.057 s, there are three waves: one right-propagating shock wave toward the right boundary, one discontinuity at the position of x=8m and one left-propagating rarefaction wave toward the left boundary, presented in Fig 4. There are no spurious oscillations in the vicinity of the discontinuous waves. Compared with the analytical solutions, the scheme can capture the exact position of discontinuity and compute the strength and speed of the shock wave, which shows the numerical scheme is high resolution.

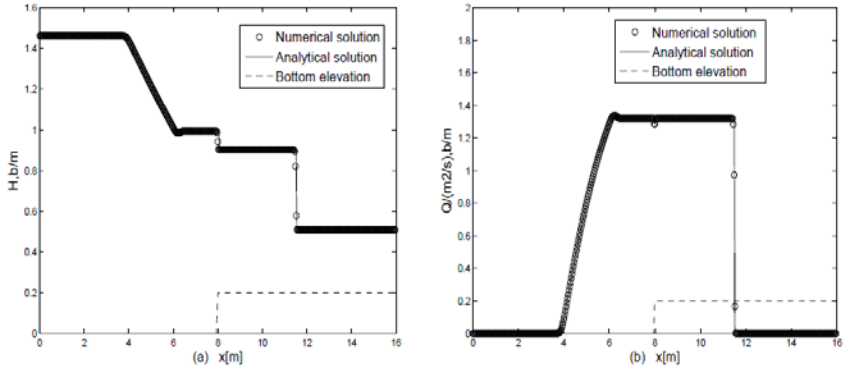

Figure 4 Numerical solutions of the water surface and discharge for dam break with a bottom step

3.2 Dam Break in the Channel with Three Humps

The numerical test proposed by Kawahara and Umetsu (Kawahara, 1986) is located in a 75m×30m rectangular channel with complicated distribution of the bottom topography as depicted, defined as

$$b(x,y)=\max\left(0,1-\frac{1}{8}\sqrt{(x-30)^2+(y-6)^2},1-\frac{1}{8}\sqrt{(x-30)^2+(y-24)^2},1-\frac{1}{8}\sqrt{(x-47.5)^2+(y-15)^2}\right) \quad (23)$$

The initial conditions are set as $u=0, v=0, H=\begin{cases}900/(16\times 30) & x\le 16m\\ 0 & x\ge 16m\end{cases}$. In this test, the solid walls are imposed at each boundary. The computational domain is discretised into 4480 triangular elements. The manning coefficient is 0.018 with CFL=0.8. At t=0, the dam immediately happens at x=16m of the channel containing $900m^3$ of water at the upstream with the dry bed at the downstream. The process of the flows for total time 300s is simulated by the numerical scheme. At T=2s, as depicted in Fig. 5(a), it is seen that the front of water wave has reached and started to climb the two smaller humps. At T=6s, as shown in Fig. 5(b), the front of the flow has reached the front of the biggest hump, with the two smaller humps submerged by water. The hump is too high for the wave to pass, so that only part of the flow can pass through the biggest hump through two sides of the biggest hump and continues to propagate downstream. Here, the pattern of the flow is very complicated as involving wet/dry front, solid wall boundary and irregular topography. At T=12s, as shown in Fig. 5(c), the wave flow is further developed and some part of the front has reached the end of the computational domain. Simultaneously, due to the interaction between the dam break wave and the humps, there generates a shock wave propagating backwards to the upstream boundary in return. In Fig. 5(d), the results at t=30s are shown. The water front has reached the right boundary. At the same time, a shock wave is created when the water front interacts the right wall boundary and moves upstream. This wave-topography-boundary interaction will continue until the momentum of moving water is dissipated by the bed friction. At t=300s, the flow becomes still with the top of the two smaller humps out of the water as shown in Fig. 5(e).

Compared with the existing results, the process of the propagation of the dam break agrees very well, so does the process of the complicated wetting and drying. Through the numerical experiment involving most obvious features of the realistic dam break problem, the numerical scheme in this paper can be extended to simulate the flows in practice.

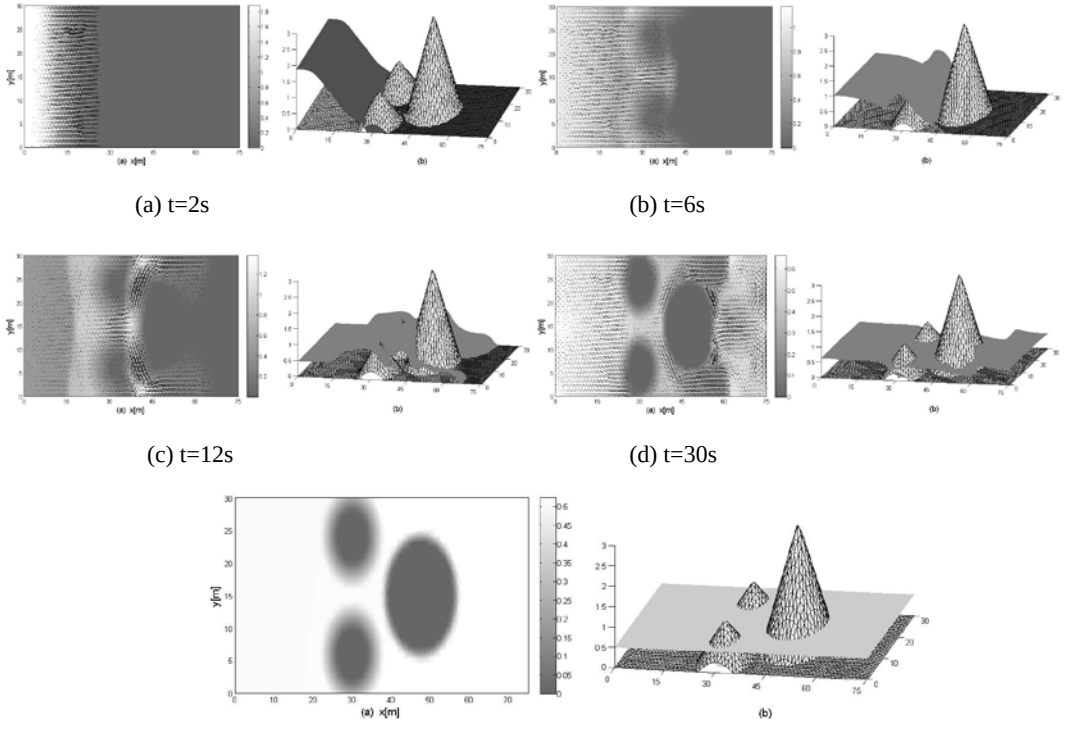

(a) t=2s (b) t=6s

(c) t=12s (d) t=30s

(e) t=300s

Figure 5 The propagation wave in dam-break over three humps at t=2,6,12,30 and 300s

4 CONCLUSION

This paper presents a well-balanced and robust numerical scheme for the 2D shallow water equations with source terms. The HLLC solver is employed to approximate the intercell numerical flux. And the MUSCL data reconstruction and second order Runge-Kutta integration are performed for space and time respectively. For the treatment of wet/dry fronts, the method of the redefinition of the discretized bottom function is performed at the wet/dry transitions. In end, the classical tests of dam break problem are presented, of which the results show that the numerical scheme is the high resolution, capture sharply the shock wave and can deal with the issue of complex domain and wet/dry front in the realistic channel.

ACKNOWLEDGEMENT

This work was supported by the National Natural Science Foundation of China (Grant No. 11102027) and Fundamental Research Fund for State Public-Benefical Scientific Institutes of CRSRI (Grant No. CKSF2013025/SL, CKSF2012010/SL, CKSF2011014/SL).

References

Alcrudo F. and Garcia-Navarro P., 1993. A high-resolution Godunov-type scheme in finite volumes for the 2D shallow water equations. Int. J. Numer. Methods in Fluids, 16, 489-505.

Castro M. J., Ferreiro A., Garcia J. A., Gonzalez J. M., Macias J., Pares C., and Vazquez-Cendon M. E., 2005. The numerical treatment of wet/dry fronts in shallow water flows: application to one-layer and two-layers systems. Mathematical and Computer Modelling, 42, 419-439.

Delis A. I., Skeels C. P. and Ryrie S. C., 2000. Evaluation of some approximate Riemann solvers for transient open channel flows. J. Hydraul. Res., 38(3), 217-231.

Godunov S. K., 1959. Finite difference methods for the computation of discontinuous solutions of the equations of fluid dynamics. Mat. Sb., 47, 271-306.

Kawahara M. and Umetsu T., 1986. Finite element method for moving boundary problems in river flow. Int. J. Numer. Methods in Fluids, 6, 365-386.

LeVeque R. J., 1998. Balancing source terms and flux gradients in high-resolution Godunov methods: the quasi-steady wave-propagation algorithm. J. Comput. Phys., 146, 346-365.

Roe P. L., 1986. Upwind differencing schemes for hyperbolic conservation laws with source terms, in Nonlinear Hyperbolic Problems, C.Carraso, P.-A.Raviart, and D.Serre, eds., Springer-Verlag, Lecture Notes in Mathematics 1270, 41-51.

Toro E. F., 2001, Shock-Capturing Methods for Free-Surface Shallow Flows. Wiley and Sons Ltd., New York.

Vignoli G., Titarev V. A. and Toro E. F., 2008. ADER schemes for the shallow water equations in channel with irregular bottom elevation. J. Comput. Phys., 227, 2463-2480.

Xing Y. and Shu C. W., 2006. High order well-balanced finite volume WENO schemes and discontinuous Galerkin methods for a class of hyperbolic systems with source term. J. Comput. Phys., 214, 567-598.

Zhao D. H., Lai H. W., Lai J. S. and Tabios III G. Q, 1996. Approximate Riemann problem slovers in FVM 2D hyraulic shock wave modeling. J. Hydr. Engrg., 122(12), 692-702.

Zhou J. G., Causon D. M., Minghan C. G. and Ingram D. M., 2001. The surface gradient method for the treatment of source terms in the shallow-water equations. J. Comput. Phys., 168, 1-25.